International Journal of Nanoelectronics and Materials
Volume 16, No. 2, April 2023 [301-312]

Ultra-wide Bandgap AlGaN Channel HEMTs for Portable Power Electronics Applications

A. Revathy[1,*], C.S. Boopathi[1]

[1]Department of Electrical and Electronics Engineering, SRM Institute of Science and Technology, Chennai-India

Received 2 August 2022, Revised 8 September 2022, Accepted 20 September 2022

ABSTRACT

AlGaN channel (E_g>3.4 eV) is the most effective method for enhancing the breakdown field of the group III-nitride based HEMTs. This work demonstrates the potential of AlGaN double channel HEMTs on Silicon carbide substrate. The device DC characteristics are investigated using numerical simulator by using drift-diffusion transport model. The AlGaN double channel HEMTs enhances the total 2DEG density due to double potential well and shows better current driving capability (I_{DS}) of 0.714 A/mm, transconductance (g_m) of 116 mS/mm, and low specific ON-resistance (R_{on}) of 3.262 Ω.mm. The AlGaN double channel HEMT on Silicon carbide substrate exhibited 680 V blocking voltage (V_{BR}) and gate field plate HEMT shows 532 V. The effective reduction in electric field at the gate edge is the major source for elevated breakdown voltage in field plate HEMTs. The superior DC characteristics indicates the proposed wide bandgap channel HEMT is suitable device for future portable power converters.

Keywords: Double channel; AlGaN; breakdown voltage; transconductance; ON resistance; high power switching

1. INTRODUCTION

Group III-nitride semiconductor materials are offering wide range of bandgaps (0.6 eV to 6.2 eV) and widely used in high power switching applications and RF amplifications [1]. GaN channel based heterostructure devices (AlGaN/GaN) are commercially available in the market for power switching and RF applications [2-4]. The technological advantages of AlGaN/GaN HEMTs, results in high critical electric field, high ON-state current, low switching loss, and high efficiency. GaN-HEMTs are widely adopted in commercial and military applications such as DC/DC converter, and DC/AC converters for automotive electronics, discrete power ICs in electronics appliances and computing, photovoltaic inverter, motor drive control, and Uninterrupted power supply for industry applications.

As the GaN channel based HEMT technology mature, ultra-wide bandgap AlGaN channel (E_G>3.4 eV) based HEMTs are the choice of semiconductor researchers for the next generation power electronics [5 -15] because AlGaN channel HEMTs exhibits 4-5 times high breakdown field than GaN channel HEMTs. Moreover, AlGaN channel also exhibited high saturation velocity [7].

Takuma Nanjo et al. demonstrated the first operation of AlGaN channel HEMTs in the year 2008 [8] and the device showed remarkable improvement in breakdown voltage. A 1 µm gate length $Al_{0.15}Ga_{0.85}N$ channel HEMT demonstrated higher breakdown voltage V_{BR} (500 V) than conventional GaN channel HEMTs [9]. A graded n++ AlGaN ohmic contact $Al_{0.75}Ga_{0.25}N$ channel HEMT demonstrated 224 V breakdown voltage [10]. The $Al_{0.65}Ga_{0.35}N$ channel HEMT on AlN buffer exhibited V_{BR} of 770 V. A hybrid Ohmic/Schottky drain contact AlGaN channel HEMT showed the breakdown voltage of 500 V for L_G = 3 µm, and L_{GD} = 6 µm [12].
The GaN capped $Al_{0.1}Ga_{0.9}N$ channel HEMT showed V_{BR} of 408 V for L_G = 1 µm and L_{GD} = 5 µm [13]. Al-rich polarization doped (PolFETs) AlGaN (Al = 0.7→0.85) channel HEMT demonstrated more

* Corresponding author: arevathynew@gmail.com

than 620 V breakdown voltage (V_{BR}) for L_G = 3.1 μm and L_{GD} = 9.6 μm [14]. A V_{BR} of 110 V was measured for L_{GD} = 3.5 μm and L_G = 0.7 μm graded AlGaN channel HEMT [15].
Despite the high V_{BR} of the reported $Al_xGa_{1-x}N$ channel-based transistors, the current driving capability is smaller than the conventional GaN binary channel due to alloy disorder scattering mechanism in AlGaN channel, which degrades the 2DEG (Two-dimensional electron gas) mobility (< 900 cm^2/v.s) [7-15] and current driving capability of AlGaN channel HEMTs. One way to improve the 2DEG density is by Al-rich AlGaN barrier HEMTs but it increases the fabrication complexity. Therefore, an alternate device design is required for further enhancing the breakdown voltage and drain current density of the AlGaN channel device. The double channel GaN HEMTs [16-17] improves the carrier density, and drain current density without limiting the carrier mobility. In spite of low breakdown voltage, the InGaN channel double based HEMT exhibited a strong coupling between the channels and showed improved drain current density [18]. AlGaN double quantum well HEMT on sapphire substrate showed an excellent carrier mobility (1130 cm^2/v.s) and breakdown performance and improved drain current density [19].

Field plate $Al_{0.1}Ga_{0.9}N$ double channel HEMTs are investigated in this work for further improving the breakdown performance of the HEMT and the results are compared with AlGaN single channel HEMTs with identical device dimensions. The device DC characteristics are investigated using TCAD numerical simulator [20]. The proposed HEMT showed a maximum of 680 V breakdown voltage and 0.714 A/mm On-state drain current.

2. AlGaN DOUBLE CHANNEL HEMTs DEVICE STRUCTURE AND NUMERICAL SIMULATION

The epi-layer of AlGaN double channel HEMTs cross section view is shown in Fig.1 and AlGaN single channel HEMTs cross section view is shown in Fig.2. A numerical study carried out for three different gate configuration such as conventional rectangular gate, field plate gate and recessed floating field plate. All three devices DC characteristics are analysed for identical device dimensions (L_G = 800 nm, L_{GD} = 1000 nm, and L_{GS} = 800 nm). A gate field plate with L_{FP} = 500 nm length used for Device B and Device C has 50 nm recess depth and 500 nm length floating field plate along with conventional gate structure. The double channel HEMT epi-stack has 23 nm $Al_{0.31}Ga_{0.69}N$ top barrier, 30 nm $Al_{0.1}Ga_{0.9}N$ top channel, 23 nm $Al_{0.31}Ga_{0.69}N$ bottom barrier and 30 nm $Al_{0.1}Ga_{0.9}N$ bottom channel on Silicon carbide substrate. Single channel HEMT epi-stack has 23 nm $Al_{0.31}Ga_{0.69}N$ barrier, 100 nm $Al_{0.1}Ga_{0.9}N$ channel and 2200 $Al_{0.1}Ga_{0.9}N$ buffer on Silicon carbide substrate. Silicon nitride passivation deposited on the device surface for avoiding surface trap states. For all the devices, source and drain electrode defined as ohmic contact and Schottky contact defined for gate terminal by setting the appropriate work function. High Al composition AlGaN channel exhibited low mobility [7-15] than GaN channels. In this work, 10 % Al-composition $Al_{0.1}Ga_{0.9}N$ channel used for improving the 2DEG mobility [7 and 19].

The HEMT structures are simulated using Atlas TCAD by using various device physics models [20] such as Boltzmann statistical model, S-R-H recombination model, nitride specific mobility models, polarization model, and impact ionization model. The bandgap (E_G), dielectric constant (Ɛ), spontaneous polarization (P_{SP}), and piezoelectric polarization (P_{PE}) of $Al_xGa_{1-x}N$ ternary material are calculated as follows [20]:

$$E_G(Al_xGa_{1-x}N) = 1.95x + 3.42(1-x) - 2.5x(1-x) \quad (1)$$
$$\in (Al_xGa_{1-x}) = 0.03x + 10.28 \quad (2)$$
$$P_{SP}(Al_xGa_{1-x}) = -0.090x - 0.034(1-x) + 0.021x(1-x) \quad (3)$$
$$P_{PE} = 2\frac{a_s - a_0}{a_0}\left(e_{31} - e_{33}\frac{C_{13}}{C_{33}}\right) \quad (4)$$

where, a_s and a_0 are lattice constants, C_{13} and C_{33} are elastic constants, and e_{31} and e_{33} are piezoelectric constants.

The total polarization (P) obtained from:

$$P = P_{SP} + P_{PE} \quad (5)$$

The induced charge density at the III-nitride heterojunction is given by:

$$\sigma = \left(P_{SP}^{bottom} - P_{SP}^{top}\right) + \left(P_{PE}^{bottom} - P_{PE}^{top}\right) \quad (6)$$

The breakdown characteristics simulation of proposed AlGaN double channel HEMTs is performed using impact ionization model. The impact ionization rate described by impact ionization coefficients ($\alpha_n,\ \alpha_p$), which accounts for number of electron-hole pair generation per unit distance [20]:

$$G = \alpha_p|J_p| + \alpha_n|J_n| \quad (7)$$

The doping and lattice temperature (T) dependent Albrecht low field mobility described as follows:

$$\mu_0(T,\ N) = \mu^{\beta_1}_{\min\left(\frac{T}{300}\right)} + \frac{(\mu_{max}-\mu_{min})\left(\frac{T}{300}\right)^{\beta_2}}{1+\left[\frac{N}{N_{ref}\left(\frac{T}{300}\right)^{\beta_3}}\right]^{\alpha\left(\frac{T}{300}\right)^{\beta_4}}}\ , \quad (8)$$

The nitride high field mobility can be obtained from the low field mobility ($\mu_0(T,\ N)$):

$$\mu = \frac{\mu_0(T,N)+v^{sat}\frac{E^{n1-1}}{E_C^{n1}}}{1+a\left(\frac{E}{E_C}\right)^{n2}+\left(\frac{E}{E_C}\right)^{n1}}\ , \quad (9)$$

The energy band details of proposed AlGaN double channel and AlGaN single channel HEMTs are plotted in Fig.3. The wurtzite III-nitride semiconductors with a wide bandgap $Al_{0.31}Ga_{0.69}N$ and narrow bandgap $Al_{0.1}Ga_{0.9}N$ creates the two-dimensional gas (2-DEG) at the interface. There are two potential wells are formed corresponding to top and bottom channel in Fig.3 (a), whereas Fig.3 (b) displays the single potential well corresponding to single channel ($Al_{0.31}Ga_{0.69}N/Al_{0.1}Ga_{0.9}N$) HEMT. The 2DEG charge details of double and single channel HEMTs are plotted in Fig.4. The upper channel 2DEG of 1.12×10^{13} cm^{-2} and lower channel 2DEG of 1×10^{13} cm^{-2} obtained for double channel HEMT. The major source for 2DEG in nitride semiconductors is donor-like surface states [21], which is closer to upper channel. This may be the major reason higher 2DEG in upper channel plotted in Fig.4(a). Fig.4(b) illustrates the 2DEG of 1×10^{13} cm^{-2} corresponding to AlGaN single channel HEMT.

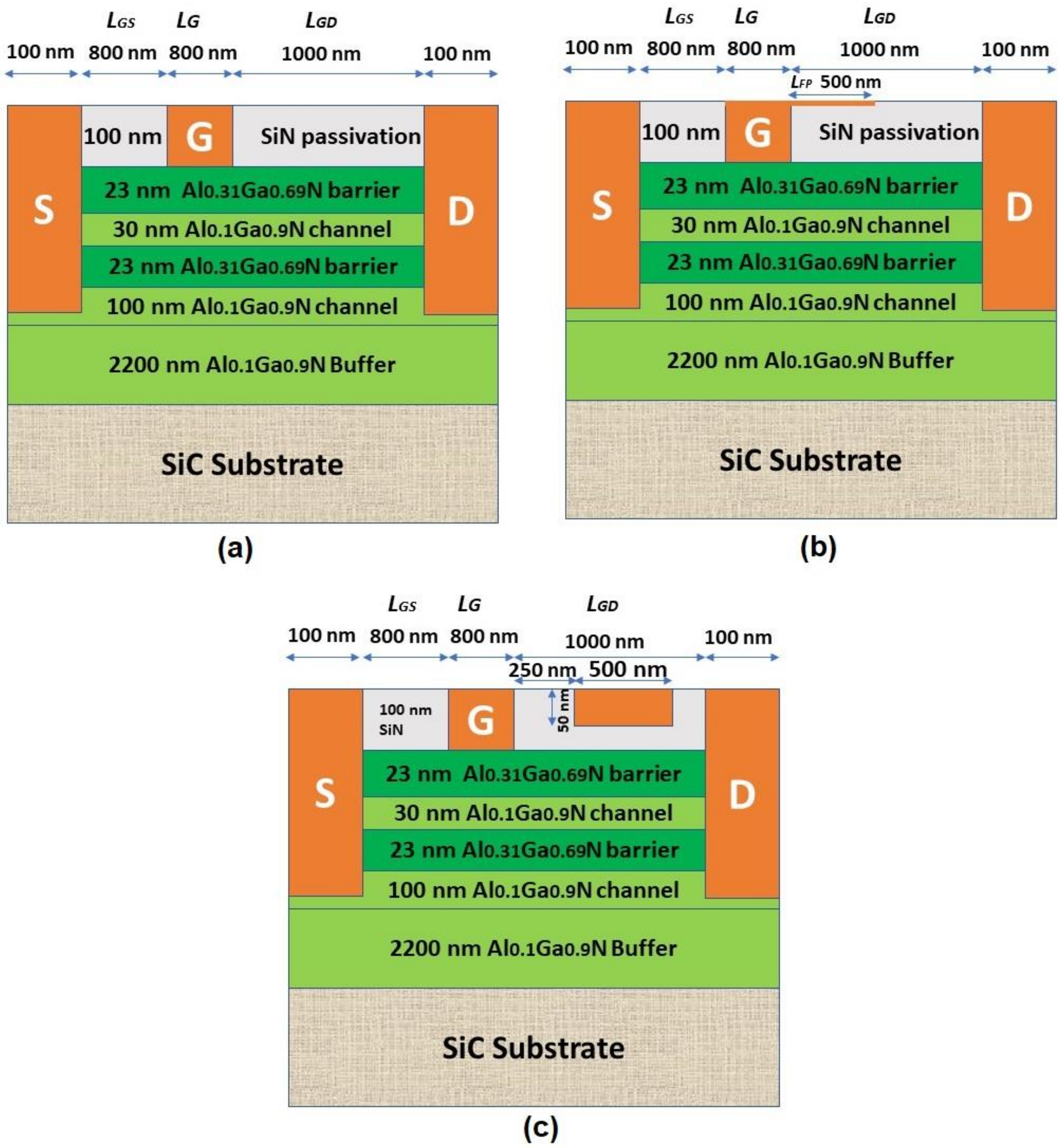

Figure 1. AlGaN double channel: (a) conventional gate, (b) Gate field plate, (c) Floating gate field plate HEMT

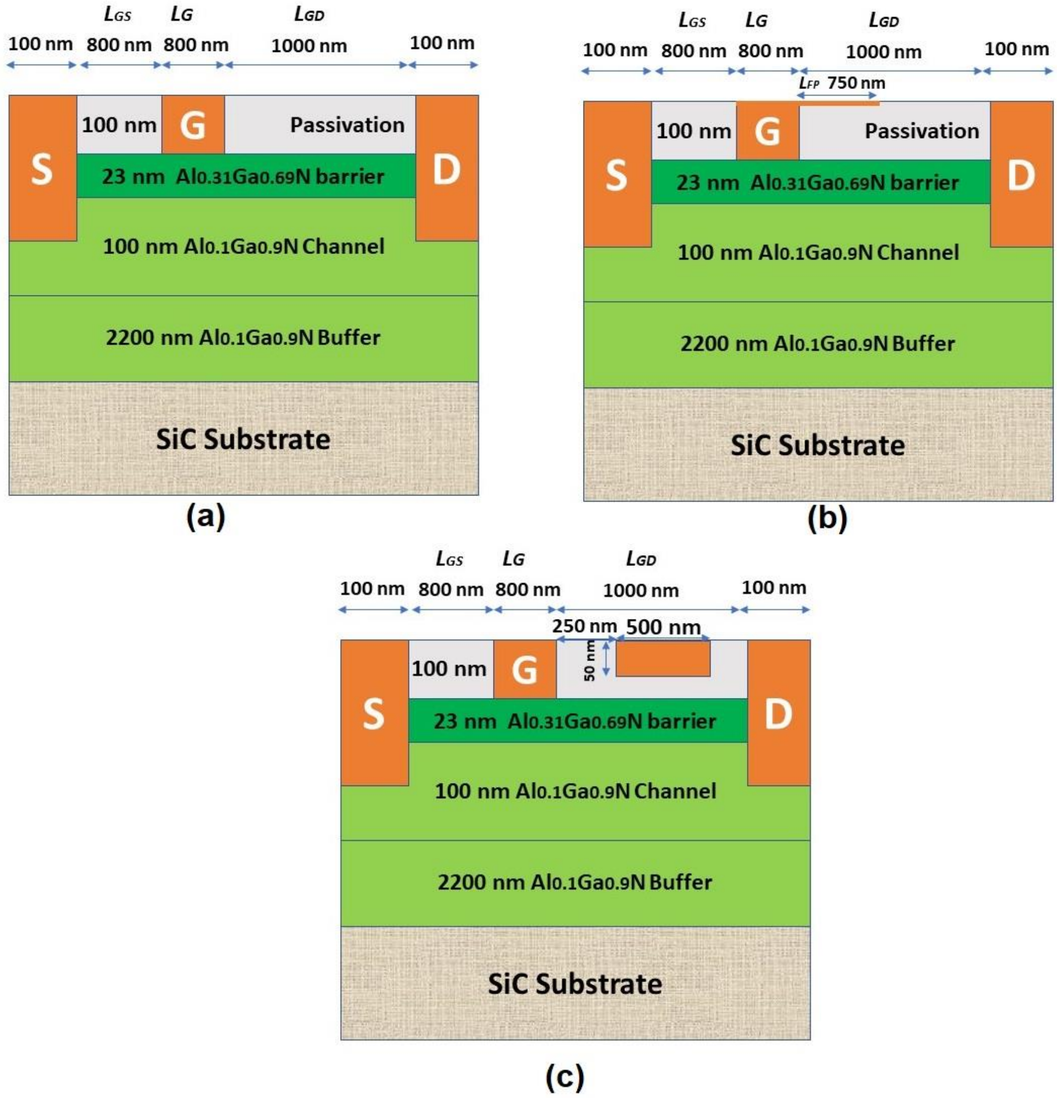

Figure 2. AlGaN single channel: (a) conventional gate, (b) Gate field plate, (c) Floating gate field plate HEMT

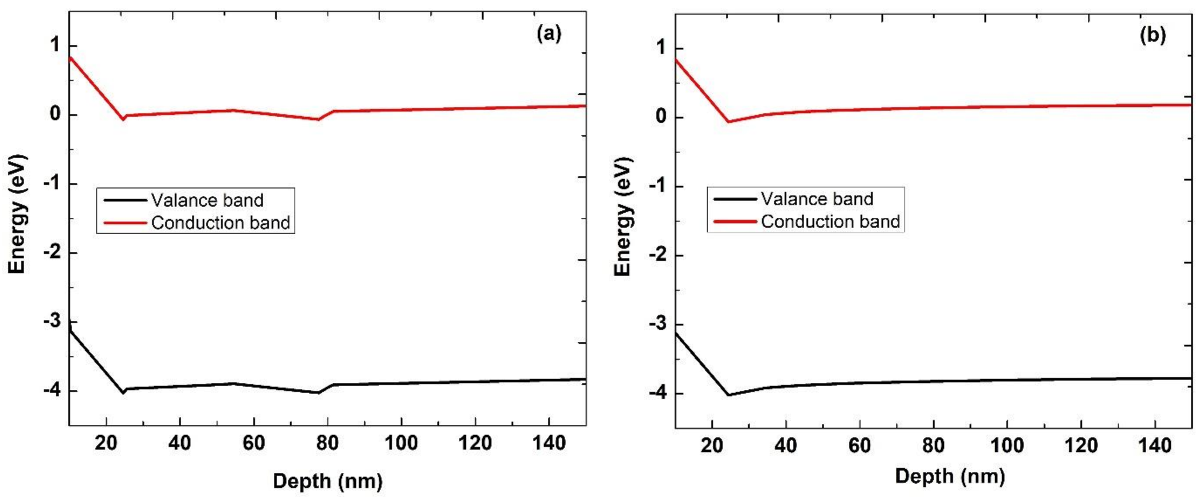

Figure 3. Band diagram of: (a) AlGaN double quantum well, (b) AlGaN single quantum well

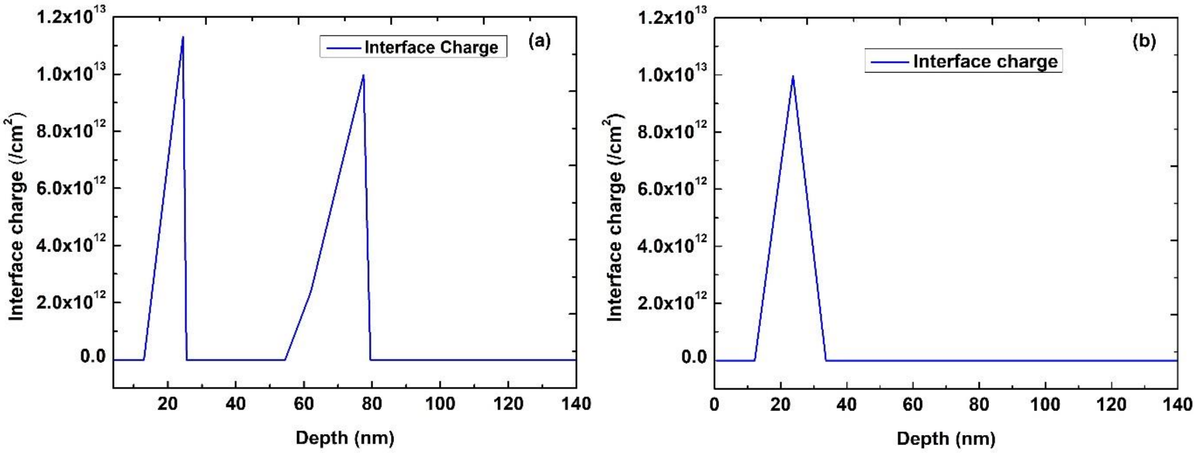

Figure 4. Interface charge details: (a) AlGaN double quantum well, (b) AlGaN single quantum well

3. RESULTS AND DISCUSSION

The proposed $Al_{0.1}Ga_{0.9}N$ double channel HEMT output characteristics is plotted in Fig.5(a) for V_{GS} = 0 V to -16 V with the step size of 2 V. The device on-state peak drain current density (I_{DS}) of 0.714 A/mm obtained at zero gate bias and the HEMT is pinched-off perfectly at -16 V gate bias. The AlGaN double channels HEMTs demonstrated this high current driving capability of proposed HEMT than existing HEMTs [8-15]. The double channel structure promotes the peak drain current density of the HEMTs by offering excellent transport properties. The on-resistance ($R_{on} = \Delta V_{DS}/\Delta I_{DS}$) of 3.262 Ω.mm is calculated from V-I curve at V_{GS} = 0 V. The V-I characteristics of $Al_{0.1}Ga_{0.9}N$ single channel HEMT is illustrated in Fig.5(b) and the HEMT exhibited I_{DS} of 0.28 A/mm and on-resistance R_{on} of 6.38 Ω.mm extracted for V_{GS} = 0 V.

Fig.6(a) illustrates the DC transfer and transconductance (g_m) characteristics of the AlGaN double quantum well device for V_{DS} = 10 V. Double quantum well HEMT showed -16 V threshold voltage and the device shows double-hump transconductance characteristics due to double quantum well as shown in Fig.6(a). The first peak g_m of 116 mS/mm exhibited by device at V_{GS} = -13.5 V and second peak g_m of 103.64 mS/mm recorded at V_{GS} = -9.5 V. Existence of double channel, more negative gate bias (V_{th}) required to deplete the 2DEG in the channels. Fig.6(b) shows the transfer characteristics of AlGaN single channel HEMT and it is clearly observed that the device showed a peak g_m of 95 mS/mm at -2.25 V gate bias. This simulation results shows the merits of AlGaN double channel over AlGaN single channel device. In order to validate our simulation models with the experimental results, TCAD simulation is performed for L_G = 0.8 μm AlGaN channel HEMT experimental work [19] and depicted in Fig.7 (a) and Fig.7 (b) for V-I and transfer characteristics respectively, which shows the accuracy of TCAD simulation against the experimental results.

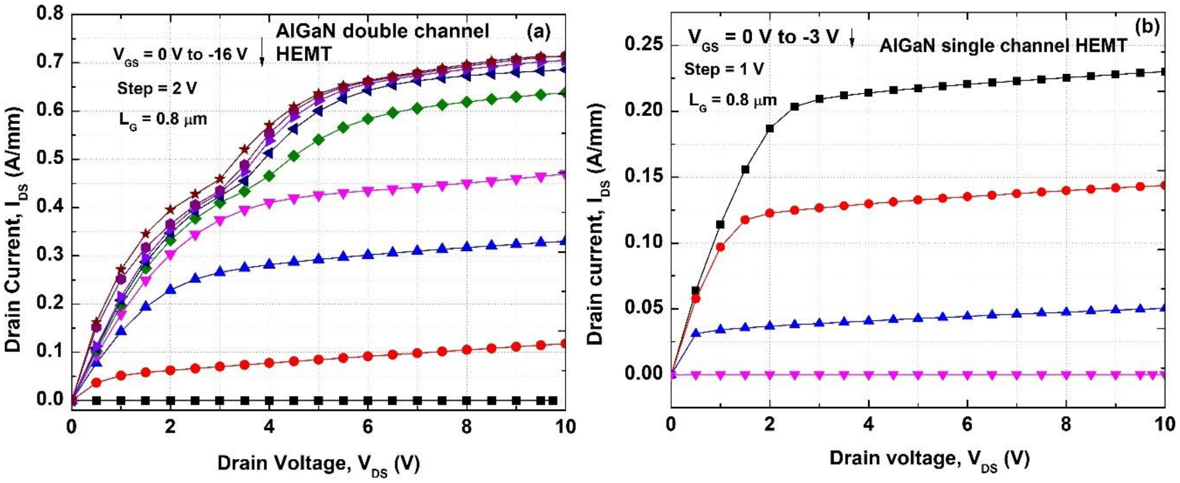

Figure 5. V-I characteristics of: (a) AlGaN double quantum well, (b) AlGaN single quantum well

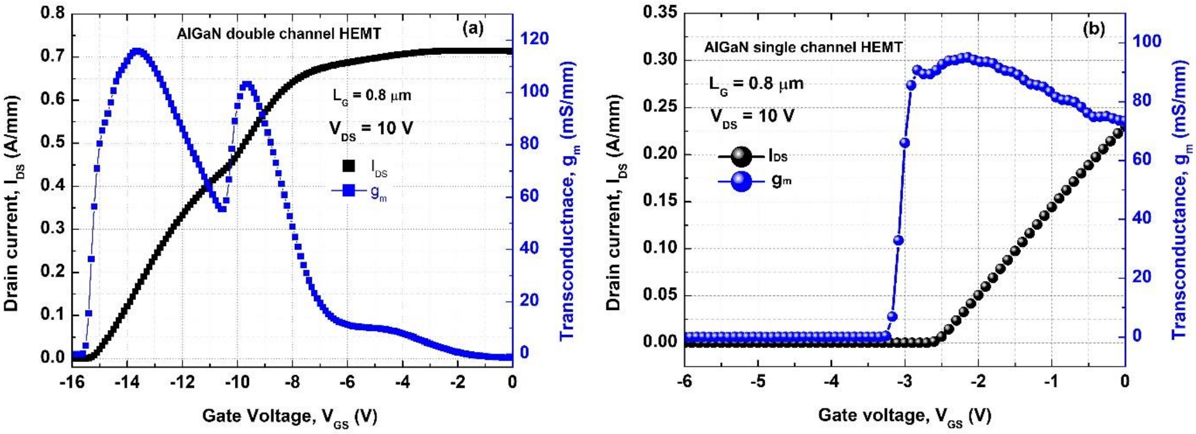

Figure 6. Transfer characteristics of: (a) AlGaN double quantum well, (b) AlGaN single quantum well

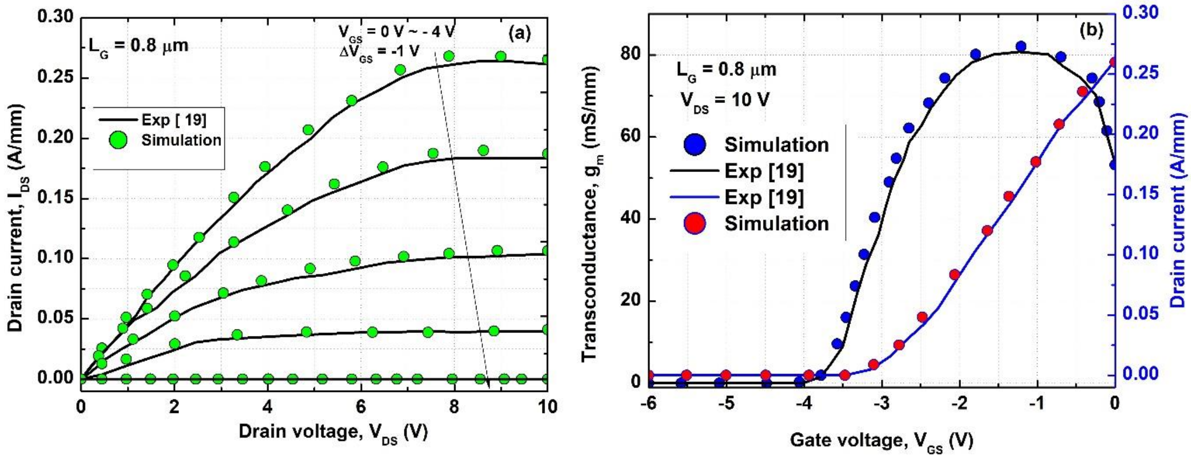

Figure 7. Validation of simulation results with experimental works of AlGaN channel HEMT [19]: (a) Typical VI characteristics, (b) Transfer characteristics

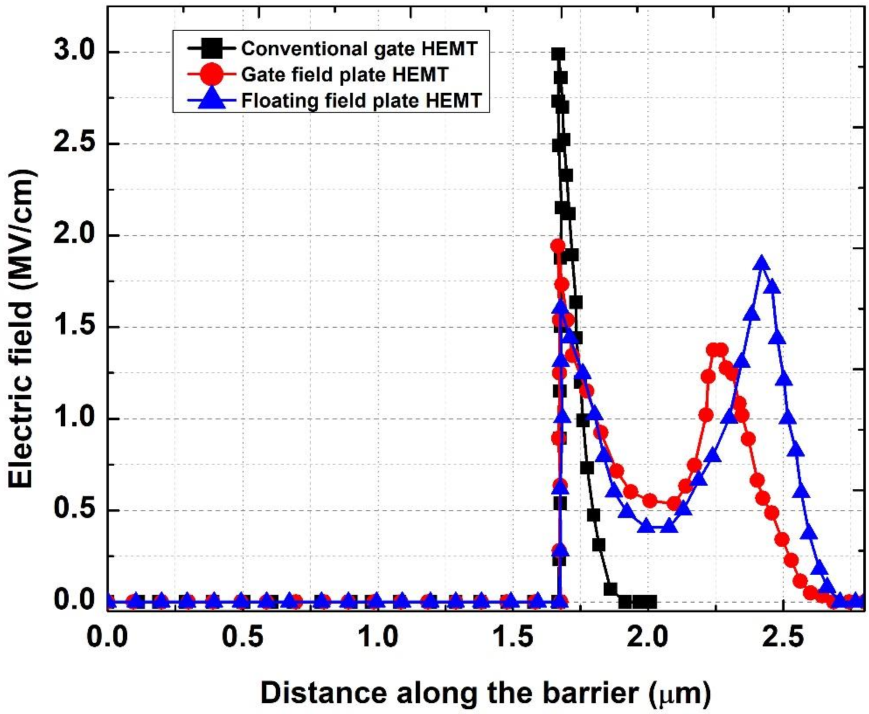

Figure 8. Electric field distribution of AlGaN double channel HEMTs

The high off-state blocking voltage (V_{BR}) along with low on-resistance (R_{on}) of the HEMTs is desirable for low loss high-power switching applications. The proposed double channel HEMTs showed a low R_{on} than single channel HEMT. The breakdown mechanism in GaN-based HEMTs mainly due to impact ionization effect, which will increase the drain current rapidly when the device is at off-state due to generation of electron-hole pairs close to the gate [22]. The impact ionization depends on the critical electric field of the channel material and peak electric field near the gate, which initiate the avalanche multiplication. The impact ionization arises due to the injection of negative charges from source region to gate region. This impact ionization contributes significantly higher drain current at the output of the HEMT.

Physics-based numerical simulation was carried out to demonstrate breakdown behaviour of AlGaN channel HEMTs using Selberherr impact ionization model [20] and it expressed as follows:

$$\alpha_n = A_n exp\left[\left(\frac{B_n}{E}\right)^{\beta_n}\right] \tag{10}$$

$$\alpha_p = A_p exp\left[\left(\frac{B_p}{E}\right)^{\beta_p}\right] \tag{11}$$

Here, α_n and α_p are electron and hole ionization rates respectively. A_n, B_n, A_p, B_p, $\beta_n$and β_p are the fitting parameters in the model.

The electric field distribution of AlGaN double channel HEMTs is plotted in Fig.8. In the conventional gate HEMT, a high electric field presence near gate edge, which initiate the impact ionization process and caused to early breakdown of the device. Introducing a gate field plate technique, modulating the electric field and suppresses the peak electric field near the gate. The recessed floating field plate further suppresses the electric field and re-shape the field distribution leads to avoid early breakdown mechanism of the HEMTs.

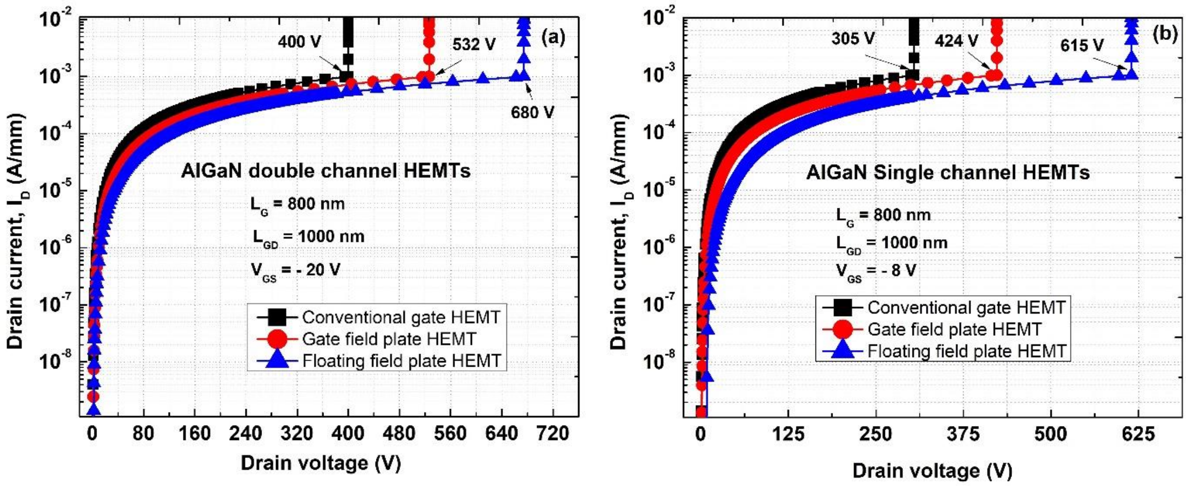

Figure 9. (a) Breakdown characteristics of AlGaN double channel HEMTs, (b) Breakdown characteristics of AlGaN single channel HEMTs

Fig.9 shows the breakdown performance of double quantum well and single quantum well HEMTs. Conventional rectangular gate double channel HEMT showed V_{BR} of 400 V as illustrated in Fig.9 (a). The corresponding logarithmic electron concentration is displayed in Fig.10(a), which depicts the width of the depletion layer of Device A. The HEMT with field plate gate reshaped the electric field and minimized the peak electric field at the drain edge of the gate as shown in Fig.8 and hence the breakdown voltage improved from 400 V to 532 V. The V_{BR} of the device also proportional to the total area (E-field) under the lobe [23] as illustrated in Fig.8 and Fig.9(a). The depletion width of Device B is higher than Device A as illustrated in Fig.10(a) and Fig.(b). Device C uses a 500 nm recessed floating field plate, which further reduces the electric field near the gate and the shape of the E-field distribution is entirely different from the previous two. The recesses floating field plate in to the SiN insulator modulates the E-field on the surface in effective manner and further extends the depletion region width as shown in Fig.10(c) due to smaller distance to the 2DEG channel and it elevates the breakdown voltage of the HEMT up to 680 V as shown in Fig.9 (a). The AlGaN single channel HEMTs with identical device dimensions (L_G = 800 nm, and L_{GD} = 1000 nm) exhibited a breakdown voltage of 305 V, 424 V, and 615 V for rectangular, gate field plate, and recessed floating field plate structure respectively.

The benchmarks of ternary ($Al_xGa_{1-x}N$) channel HEMTs breakdown voltage are presented in the Table 1. The proposed AlGaN double channel HEMT showed an improved breakdown voltage than existing reported works for the minimum device dimensions. And therefore, the recessed floating field plate AlGaN double channel HEMTs provides the viable solution for next generation power electronics applications.

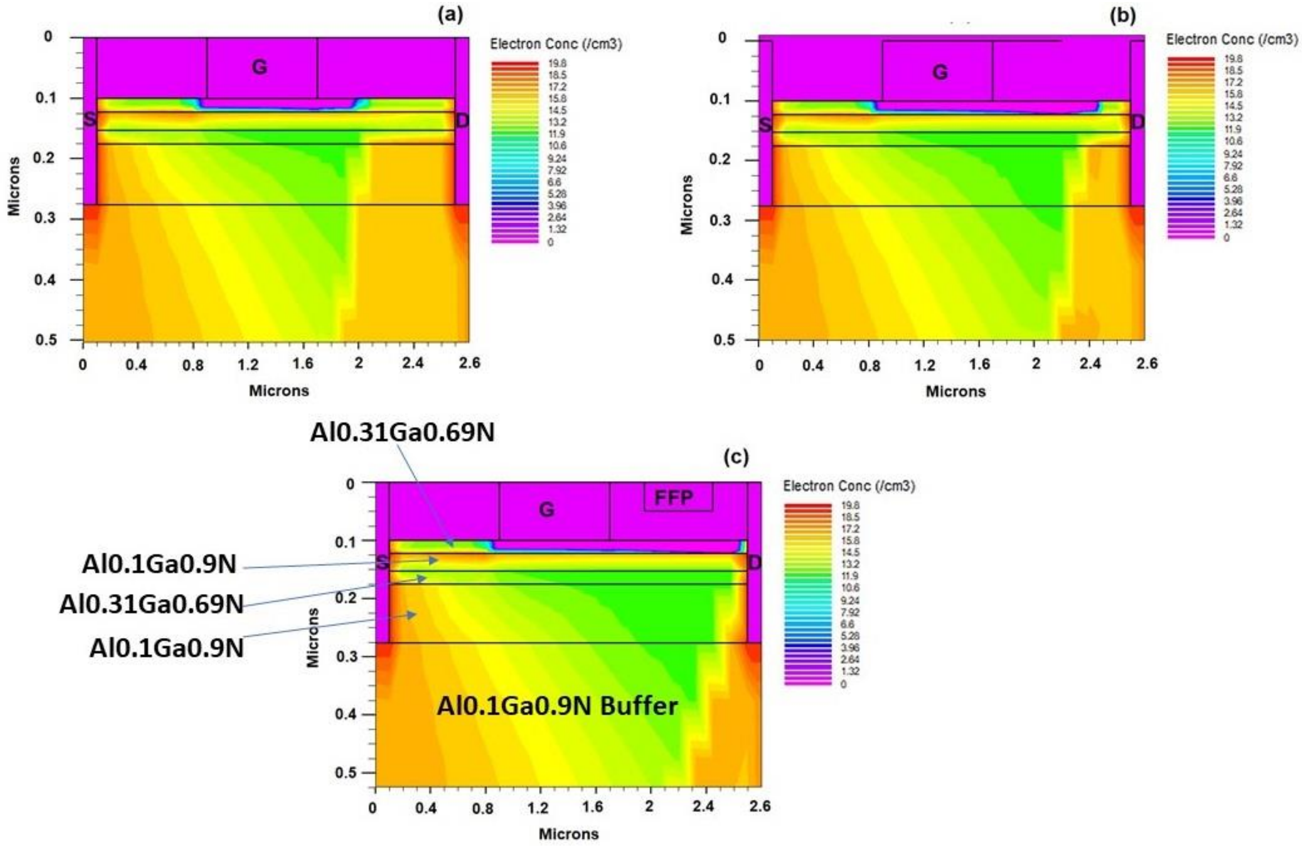

Figure 10. logarithmic electron concentration of AlGaN double channel HEMTs: (a) conventional gate, (b) Gate field plate, (c) Floating gate field plate at breakdown condition.

Table 1. Summary of wide bandgap channel heterostructure devices breakdown performance

S.No	Ref.No	Gate length (L_G) in µm	Gate to drain distance (L_{GD}) in µm	Breakdown voltage (V_{BR}) in V
1	[9]	1	3	500
2	[10]	0.7	1.1	224
3	[11]	1.8	9	770
4	[12]	3	6	500
5	[13]	1	5	408
6	[14]	3.1	9.6	620
7	[15]	0.7	3.5	110
8	[19]	0.8	1	143.5
9	**This work [Floating field plate]**	**0.8**	**1**	**680**

4. CONCLUSION

The DC characteristics of L_G = 0.8 µm AlGaN double channel HEMTs has been investigated using numerical simulation. Device showed an improved high on-state current, and transconductance due to double quantum well structure. The floating field plate HEMT effectively modulates the E-field and elevated the V_{BR} of the device 50 % more than rectangular gate HEMT and 25 % more than a field plate gate structure. And also, the proposed HEMT showed a very low ON-resistance of 3.262 Ω.mm. Therefore, the recessed floating field plate AlGaN double channel HEMTs are suitable for high power-low power loss applications to improve the power performance with minimum transistor size.

ACKNOWLEDGEMENTS

The authors acknowledge the SRM Institute of Science and Technology, Chennai, India-603 203 for providing the support and facility to carry out this research work.

REFERENCES

1. Zeng F, An JX, Zhou G, Li W, Wang H, Duan T, Jiang L, Yu H, "A Comprehensive Review of Recent Progress on GaN High Electron Mobility Transistors: Devices, Fabrication and Reliability", *Electronics*, 7(12), (2018), pp.377. https://doi.org/10.3390/electronics7120377.
2. E. A. Jones, F. F. Wang and D. Costinett, "Review of Commercial GaN Power Devices and GaN-Based Converter Design Challenges," *IEEE Journal of Emerging and Selected Topics in Power Electronics*, 4(3), (2016), pp. 707-719. https://doi.org/10.1109/JESTPE.2016.2582685.
3. Flack, T.J., Pushpakaran, B.N. & Bayne, S.B, "GaN Technology for Power Electronic Applications: A Review", *Journal of Elec Materi,* 45, (2016), pp.2673–2682. https://doi.org/10.1007/s11664-016-4435-3.
4. K. Husna Hamza, D. Nirmal, "A Review of GaN HEMT Broad Band Power Amplifiers", *International Journal of Electronics and Communications, 116* (2019), https://doi.org/10.1016/j.aeue.2019.153040.
5. Y. Wu *et al*., "More Than 3000 V Reverse Blocking Schottky-Drain AlGaN-Channel HEMTs With >230 MW/cm^2 Power Figure-of-Merit," *IEEE Electron Device Letters*, 40 (11), (2019), pp. 1724-1727. https://doi.org/10.1109/LED.2019.2941530.
6. Michael E. Coltrin, Albert G. Baca and Robert J. Kaplar , "Analysis of 2D Transport and Performance Characteristics for Lateral Power Devices Based on AlGaN Alloys", ECS Journal of Solid State Science and Technology, 6(11), (2017), https://doi.org/10.1149/2.0241711jss.
7. M. Farahmand *et al*., "Monte Carlo simulation of electron transport in the III-nitride wurtzite phase materials system: binaries and ternaries," *IEEE Transactions on Electron Devices*, 48(3), (2001), pp. 535-542. https://doi.org/10.1109/16.906448.
8. Takuma Nanjo, Misaichi Takeuchi, Muneyoshi Suita, Yuji Abe, Toshiyuki Oishi, Yasunori Tokuda and Yoshinobu Aoyagi, "First Operation of AlGaN Channel High Electron Mobility Transistors", The Japan Society of Applied Physics Applied Physics Express, 1(1), 2008. https://doi.org/10.1143/APEX.1.011101.
9. T. Nanjo *et al*., "AlGaN Channel HEMT With Extremely High Breakdown Voltage," *IEEE Transactions on Electron Devices*, 60(3), (2013), pp. 1046-1053. https://doi.org/10.1109/TED.2012.2233742.
10. Sanyam Bajaj, Fatih Akyol, Sriram Krishnamoorthy, Yuewei Zhang, and Siddharth Rajan, "AlGaN channel field effect transistors with graded heterostructure ohmic contacts", Appl. Phys. Lett. 109(133508), (2016); https://doi.org/10.1063/1.4963860.
11. S. Muhtadi *et al*., "High Electron Mobility Transistors With $Al_{0.65}Ga_{0.35}N$ Channel Layers on Thick AlN/Sapphire Templates," *IEEE Electron Device Letters*, 38(7), (2017), pp. 914-917. https://doi.org/10.1109/LED.2017.2701651.
12. W. Zhang, J. Zhang, M. Xiao, L. Zhang and Y. Hao, "High Breakdown-Voltage (>2200 V) AlGaN-Channel HEMTs With Ohmic/Schottky Hybrid Drains," *IEEE Journal of the Electron Devices Society*, 6, (2018), pp. 931-935. https://doi.org/10.1109/JEDS.2018.2864720.
13. M. Xiao *et al*., "High Performance $Al_{0.10}Ga_{0.90}N$ Channel HEMTs," *IEEE Electron Device Letters*, 39(8), (2018), pp. 1149-1151, https://doi.org/10.1109/LED.2018.2848661.
14. Andrew M. Armstrong, Brianna A. Klein, Albert G. Baca, Andrew A. Allerman, Erica A. Douglas, Albert Colon, Vincent M. Abate, and Torben R. Fortune, "AlGaN polarization-doped field effect transistor with compositionally graded channel from Al0.6Ga0.4N to AlN", Appl. Phys. Lett. 114(052103), (2019). https://doi.org/10.1063/1.5058263.

15. Shahadat H. Sohel1, Andy Xie, Edward Beam, Hao Xue, Towhidur Razzak, Sanyam Bajaj, Sherry Campbell, Donald White, Kenneth Wills, Yu Cao, Wu Lu, and Siddharth Rajan, "Improved DC-RF dispersion with epitaxial passivation for high linearity graded AlGaN channel field effect transistors", Applied Physics Express, 13(036502), (2020). https://doi.org/10.35848/1882-0786/ab7480.
16. Chu R, Zhou Y, Liu J, Wang D, Chen KJ, Lau KM, "AlGaN-GaN double-channel HEMTs", IEEE Trans Electron Devices, 52(4), (2005), pp.438-446. https://doi.org/10.1109/TED.2005.844791.
17. X. Wang, W. Hu, X. Chen, and Wei Lu, "The Study of Self-Heating and Hot-Electron Effects for AlGaN/GaN Double-Channel HEMTs", IEEE Trans.Electron Devices, 59(5), (2012), pp.1393-1401. https://doi.org/10.1109/TED.2012.2188634.
18. Yachao Zhang, ZhiZhe Wang, Rui Guo, Ge Liu, Shengrui Xu, Weimin Bao, Jincheng Zhang, and Yue Hao, "High performance InGaN double channel high electron mobility transistors with strong coupling effect between the channels", Appl. Phys. Lett. 113(233503), (2018). https://doi.org/10.1063/1.5051685.
19. Y. Zhang et al, "High-Performance AlGaN Double Channel HEMTs with Improved Drain Current Density and High Breakdown Voltage", Nanoscale Research Letters. 15(114), (2020).
20. SILVACO Int. ATLAS User's Manual; Device Simulation Software: Santa Clara, CA, USA, 2016; Available online: https://www.silvaco.com.
21. Smorchkova IP, Elsass CR, Ibbetson JP, Vetury R, Heying B, Fini P, Haus E, DenBaars SP, Speck JS, Mishra UK, "Polarization-induced charge and electron mobility in AlGaN/GaN heterostructures grown by plasma-assisted molecular-beam epitaxy", J Appl Phys, 86(4521), (1999).
22. A. Berzoy, C. R. Lashway, H. Moradisizkoohi and O. A. Mohammed, "Breakdown voltage improvement and analysis of GaN HEMTs through field plate inclusion and substrate removal," *2017 IEEE 5th Workshop on Wide Bandgap Power Devices and Applications (WiPDA)*, pp. 138-142, (2017). https://doi.org/10.1109/WiPDA.2017.8170536.
23. S. Karmalkar and U. K. Mishra, "Enhancement of breakdown voltage in AlGaN/GaN high electron mobility transistors using a field plate," *IEEE Transactions on Electron Devices*, 48(8), (2001), pp. 1515-1521. https://doi.org/10.1109/16.936500.